Journal of Energy Storage 52 (2022) 105016

Contents lists available at ScienceDirect

Journal of Energy Storage

journal homepage: www.elsevier.com/locate/est

Research papers

Modified Plett-model for modeling voltage hysteresis in lithium-ion cells

Dominik Wycisk [a,b,*], Marc Oldenburger [a], Marc Gerry Stoye [a], Toni Mrkonjic [a], Arnulf Latz [b]

[a] Mercedes-Benz AG, Neue Staße 95, 73230 Kirchheim unter Teck, Germany
[b] Ulm University, Albert-Einstein-Allee 47, 89091 Ulm, Germany

ARTICLE INFO

Keywords:
Lithium-ion battery
Voltage hysteresis
Plett-model
Silicon–graphite anode

ABSTRACT

Lithium-ion cells, especially anode materials like graphite or silicon, exhibit a charge-direction dependent voltage hysteresis. In literature, several approaches exist to model this effect. This paper aims at showing modifications to the so called Plett-model. It will be shown that the specific slope of the transition between charge and discharge OCV curves can be linked to the slope of the OCV curves themselves. This leads to a significant reduction in measurement and parameterization time. Furthermore, this paper features the application of the improved model to composite electrodes. The separation of the contributions of graphite and silicon leads to an improved modeling of the total voltage hysteresis.

1. Introduction

Li-ion batteries become more and more important for transport applications. To achieve higher ranges, new active materials are being investigated to increase energy density of Li-ion cells. One possible material for anodes of Li-ion cells is silicon. Featuring a theoretical capacity of 3579 $\frac{\text{mAh}}{\text{g}}$, the energy density can be increased by over 30% in comparison to state of the art Li-ion cells with graphite anodes [1]. The disadvantages of silicon as an anode material are high volume expansion of up to 300% [2,3] over a complete lithiation, causing potential particle- or SEI-cracking and therefore higher capacity fade. Another severe disadvantage is the big voltage hysteresis of over 200 mV between lithiation and delithiation (compared to about 30 mV for graphite) (see Fig. 2(b)). Also, current state of the art electrode materials like graphite or two-phase materials like lithium iron phosphate (LFP) or lithium titanate oxide (LTO) exhibit a non-negligible open-circuit voltage (OCV) hysteresis dependency due to the charge/discharge-history [4]. A brief overview over different explanations for the hysteresis in Li-ion cells is given in Section 2.1.

For the application of Li-ion batteries in electric vehicles, a correct estimation of the state of charge (SOC) is important. This enables a reliable prediction of the remaining range. One way to estimate the correct SOC is to use the OCV vs. SOC dependency. However, because of the described voltage hysteresis, the estimation is difficult [5,6]. To model the effect of voltage hysteresis, different mathematical models have been described in literature [7]. The models can be divided into operator-based like the Preisach model [8,9] and differential equation models like the one described by Plett et al. [10–13] or by Baker et al. [14]. In this article modifications for the Plett-model are described, which enables faster parameterization with already given measurement values. In literature, often so called First-Order-Reversal (FOR) branches (see Section 3) are used to parameterize the Plett-model [15]. To achieve a sufficient accuracy, huge measurement effort needs to be taken. To reduce the measurement effort, we take into account that the information about the hysteresis transitions is already included in the charge and discharge OCV curves of the cell. Furthermore, our modifications achieve a significant increase in modeling accuracy. The modifications can be adapted for all common cell chemistries, as will be shown for graphite, silicon and silicon–graphite composite anode cells with NMC cathodes and a graphite/LFP cell.

2. Theoretical background

2.1. Origin of hysteresis in Li-ion cells

Hysteresis describes a phenomenon where the state of a system is dependent on its history. Li-ion cells exhibit several hysteresis effects [16,17]. In this work, we focus on the OCV hysteresis. From a thermodynamic point of view, there is only one equilibrium potential for a material at a given SOC and therefore it is not history-dependent. Perfect equilibrium is achieved, when the system is in the state of its lowest total Gibbs free energy [18]. In reality, a perfect equilibrium state is difficult to achieve, as the time constants of the processes can be very long. These processes can be overpotentials due to external current flow like charge-transfer or diffusion in the liquid and solid phase. The time-constants of these effects are in the range of seconds up to hours for diffusion inside the particles [16]. Inhomogeneities perpendicular to

* Corresponding author at: Mercedes-Benz AG, Neue Staße 95, 73230 Kirchheim unter Teck, Germany.
E-mail address: dominik.wycisk@mercedes-benz.com (D. Wycisk).

https://doi.org/10.1016/j.est.2022.105016
Received 1 February 2022; Received in revised form 14 April 2022; Accepted 28 May 2022
Available online 14 June 2022

the electrode coating or in-plane in the electrode can further increase the relaxation times [19]. Another aspect is the influence of the anode overhang [20]. These relaxation effects can also be superimposed by ageing or self-discharge [21]. Therefore, the measured OCV cannot be directly treated as the equilibrium potential [22]. Due to sufficient, but not infinite, rest time after the current flow, all the effects shown in this paper are therefore measureable OCV hysteresis effects (i. e. diffusion overpotentials can be neglected) and not necessarily thermodynamic equilibrium potential effects (i.e. system in its lowest total Gibbs free energy). For this reason, the OCV hysteresis is an important aspect that needs to be considered in the battery management system (BMS).

In literature, the effect of OCV hysteresis was described for different materials. For example, the cathode material LFP exhibits a voltage hysteresis of about 20 mV [4]. Srinivasan and Newman [23] explained this behavior with a so called *shrinking core model*. In this model representation, while lithiation of a $FePO_4$ particle, a lithium-rich shell grows, while the empty core is shrinking with a sharp phase boundary between both phases. In case of delithiation of a fully lithiated particle, a shrinking lithium-rich core stays until full delithiation. Therefore, the corresponding OCV of the particle differs dependent on the history how the current SOC was set. Another explanation for the hysteresis in LFP materials is given by Dreyer et al. [4]. They describe the hysteresis in the two-phase material as a multi-particle effect. Because of a non-monotonic chemical potential, particles in a multi-particle ensemble are rather charged one after another instead of being charged simultaneously. This also leads to a path-dependent lithiation/delithiation which results in different OCVs.

For graphite, Mercer et al. [22] showed with First-Principles calculation that different history-dependent metastable states can be observed. They also show that the difference between the lithiation and delithiation OCV curves does not vanish at elevated temperatures of up to 50 °C.

As already mentioned, silicon shows a big OCV hysteresis of over 200 mV. A possible explanation is given by Sethuraman et al. [24]. In this paper, the correlation between the OCV hysteresis and the mechanical stress of a silicon thin-film is shown. With the usage of the Larche–Cahn potential, which describes the mechanical stress-dependency of the chemical potential of lithium in solid solutions, they calculate the influence of the mechanical stress of up to 62 $\frac{\text{mV}}{\text{GPa}}$. In their measurements, the observed influence of the mechanical stress is even higher with values between 100 $\frac{\text{mV}}{\text{GPa}}$ and 125 $\frac{\text{mV}}{\text{GPa}}$, which can explain a significant part of the measured voltage hysteresis. Jiang et al. [25] explain that the voltage hysteresis in silicon is path-dependent and an asymmetry arises from asymmetric reaction pathways. Another possible explanation can be the breaking of Si-Bonds [26].

It can be seen that different active-materials for Li-ion cells show OCV hysteresis and no single reason can be given for the explanation of the measured effects.

2.2. Derivation of the Plett-model

The Plett-model was originally published by Plett et al. in [10–13]. The model is based on a differential equation, which describes the current normalized hysteresis state $h(z, t)$. The differential equation is a differential equation in SOC as the transition between both OCVs is not time, but SOC-dependent.

The model separates the hysteresis H from the OCV itself. This means, that the model only describes the hysteresis behavior between the upper and lower OCV curve. The mean OCV curve OCV_{mean} has to be considered separately. The cell voltage is then defined as:

$$U_{\text{Cell}} = OCV_{\text{mean}}(z) + H(z) \cdot h(z,t) - \eta \tag{1}$$

with OCV_{mean} as the average of both OCV curves, $H(z)$ as a half of the hysteresis between the two OCV curves for a given SOC z and $h(z, t)$ is the hysteresis state between −1 and 1. η describes all overpotentials (see Section 2.1). The models used in this paper do not take overpotentials into account, as all comparison points for the model validation are measured after several hours of rest time after current flow (see Section 3). In Fig. 1 a schematic overview for the Plett-model is presented.

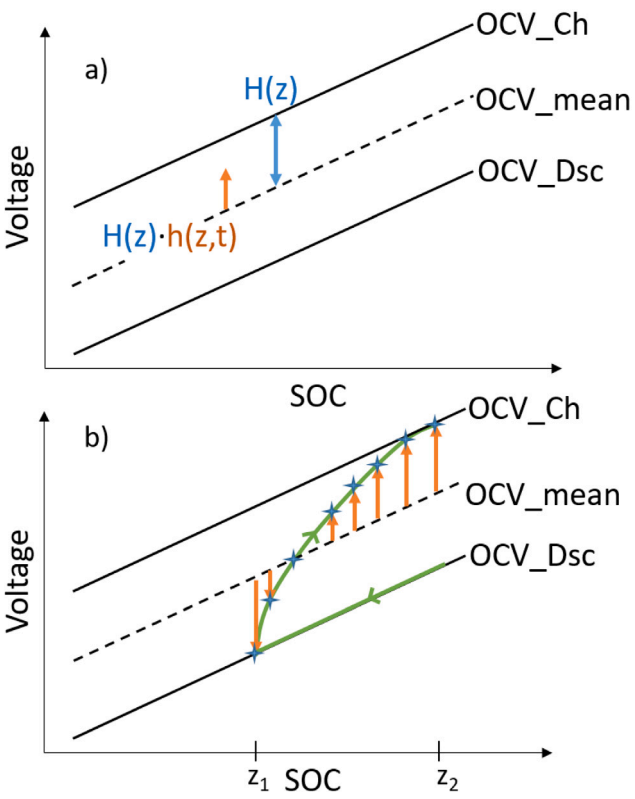

Fig. 1. (a) Schematic overview for the description of the Plett-model parameter. The difference between the mean OCV curve and the charge or discharge OCV curve is the absolute hysteresis value $H(z)$ (blue double-arrow). An exemplary hysteresis state $h(z, t)$ multiplied with the absolute hysteresis value H at the current SOC z is shown in orange. (b) Schematic transition (called FOR-branch) from discharge OCV to charge OCV (green, blue crosses: discrete values of the FOR-branch like in measurements). The orange arrows describe the hysteresis state h at different SOCs throughout the transition. All the voltages described in this schematic are OCV values. (For interpretation of the references to color in this figure legend, the reader is referred to the web version of this article.)

The differential equation for the current hysteresis state h(z,t) is given as:

$$\frac{\mathrm{d}h(z,t)}{\mathrm{d}z} = k(z)\left(1 - \operatorname{sgn}\left(\frac{\mathrm{d}z(t)}{\mathrm{d}t}\right) h(z,t)\right) \tag{2}$$

where t is the time, z(t) the state of charge, $k(z)$ the rate of decay of the hysteresis transition between the envelope curves and sgn the signum function (sign of the change of the rate of decay (either +1, 0 or −1)).

To use this model, it needs to be converted to a differential equation in time. To achieve this, Eq. (2) is multiplied by $\frac{\mathrm{d}z}{\mathrm{d}t}$ on both sides.

$$\frac{\mathrm{d}h(z,t)}{\mathrm{d}z} \cdot \frac{\mathrm{d}z}{\mathrm{d}t} = k(z)\left(1 - \operatorname{sgn}\left(\frac{\mathrm{d}z(t)}{\mathrm{d}t}\right) h(z,t)\right) \cdot \frac{\mathrm{d}z}{\mathrm{d}t} \tag{3}$$

By replacing $\frac{\mathrm{d}z}{\mathrm{d}t}$ with $\frac{I(t)}{Q_{\text{Cell}}}$ this further reduces to:

$$\frac{\mathrm{d}h(z,t)}{\mathrm{d}t} = \left(\frac{k(z) \cdot I(t)}{Q_{\text{Cell}}}\right)\left(1 - \operatorname{sgn}\left(\frac{\mathrm{d}z(t)}{\mathrm{d}t}\right) h(z,t)\right) \tag{4}$$

with Q_{Cell} as the capacity of the cell and $I(t)$ as the current.

To parameterize this model, the OCV in charge and discharge direction has to be measured. The parameter for the rate of decay $k(z)$ of the hysteresis needs to be fitted to the measurements. For this purpose, first-order reversal branches (FOR-branches) are often used, which describe a cycling of the cell with a depth of discharge (DOD) of < 100%.

Table 1
Overview of cells. (Si stands for silicon and Gr stands for graphite). The anode composition is given capacity-wise.

Name	Active mat.	Cell design	Nom. capa/Ah
Cell A	100% Gr	pouch	43
Cell B	30% Si/70% Gr	prismatic	80
Cell C	100% Si	pouch	3.5
Cell D	100% Gr/LFP	cylindrical	3.6

This means, that for example 10% SOC is set in discharge direction (Discharge from 100% SOC to 10% SOC). After a sufficient rest time the OCV is measured. Thereafter, the SOC is step-wise increased in 1% -steps again until the charge-OCV curve is reached (see Section 3). After each step, the OCV of the cell is measured. These measurement points together are called one FOR-branch. The parameter $k(z)$ in the model is then fitted to the measurement data to minimize the error between the model and the measurement data. In Fig. 1(b) an exemplary FOR-branch is shown, where a SOC z_1 is set in discharge direction. At this point, the cell is charged again and the OCV of the cells transitions from the discharge to the charge OCV. The orange arrows in the figure show exemplary output values of the model for different SOCs throughout the transition.

To describe the SOC-dependency of $k(z)$, multiple FOR-branches with varying DOD need to be measured, which increases the time for measurements and parameterization. In [15] the authors compare different parameterization possibilities for the Plett-model for a silicon-anode. They compare a parameter-set with a constant parameter k (no variation over SOC) and a constant absolute hysteresis H against a parameter-set with a variable parameter k over SOC and a variable absolute hysteresis H over SOC. They fitted k and H to 20 FOR-branches, which they measured by using a constant C/10 charge/discharge current without relaxation phases. The variable parameter-set reduces the error (RMSE) of the model from 45.4 mV to 18.3 mV (−59.1%). The measurement of 20 FOR-branches took over 200 h, which would be even worse when adding relaxation phases to measure the OCV points.

In this work, we present improvements where this parameter $k(z)$ needs to be fitted only once for a given cell chemistry and only for one FOR-branch.

3. Experimental

For measurement purposes, four different cells with different active materials are used. As NMC exhibits only a neglectable small hysteresis in the range of 1–2 mV, only the anode composition is displayed for the first three cells in Table 1. Cell type D has a LFP cathode, which has a measurable OCV hysteresis. All cells are begin of life (BoL) at a state of health (SOH) of 100%.

In most of the cases, measurement time often needs to be minimized. For the measurement of the OCV different relaxation times are used in literature varying from 1 h [27] up to 4 h [28]. In this work a variable relaxation is used, dependant on the rate of change of voltage relaxation. For all cell types, an OCV measurement is conducted according to the following procedure:

1. Charge to 100% SOC
2. Step Discharge in 2% SOC steps until $U_{\text{cutoff, min}}$ (pause between steps see step 3)
3. Relaxation (min. 2 h, max. 10 h, $\frac{dU}{dt} < 1\ \frac{\text{mV}}{\text{h}}$)
4. Step Charge in 2% SOC steps until $U_{\text{cutoff,max}}$ (pause between steps see step 5)
5. Relaxation (min. 2 h, max. 10 h, $\frac{dU}{dt} < 1\ \frac{\text{mV}}{\text{h}}$)

The OCV curves can be seen in Fig. 2. Cell type A, which has a graphite anode, shows the smallest hysteresis between the OCV after charging and discharging. Cell type B exhibits a higher hysteresis in the range between 0% and 50% SOC. This results from the higher potential of silicon in comparison to graphite. Therefore, in lower SOC-ranges, where the anode potential is higher, mostly silicon particles are lithiated or delithiated. At higher SOCs mostly graphite is used, which exhibits only a small hysteresis of about 30 mV. For cell type C, a hysteresis of about 150 mV with a peak of up to 200 mV can be seen over almost the complete SOC-range.

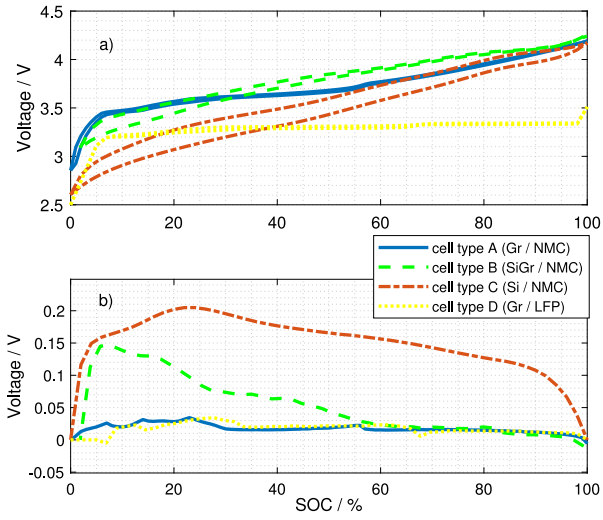

Fig. 2. (a) OCV curves of the cells. (b) Hysteresis curves of the cells.

Table 2
Exemplary description of measured FOR-branches to validate the model. For one FOR-branch, the given SOC steps are set according to the table. The step sequence ends, when the opposite OCV is reached. After each step, the OCV of the cell is measured. All relaxed voltages of the step sequence build one FOR-branch.

FOR-branch	SOC step sequence
10% CaD	100 - 20 - 15 - 10 - 11 - 12 - 13 ...
30% CaD	100 - 40 - 35 - 30 - 31 - 32 - 33 ...
65% CaD	100 - 75 - 70 - 65 - 66 - 67 - 68 ...
40% DaC	0 - 30 - 35 - 40 - 39 - 38 - 37 ...
...	...

To validate the model, FOR-branches are measured in both directions (see Table 2 and Fig. 1(b)). The following table displays the sequence of SOC values, which are set each one by one. After each SOC step, the OCV is measured. These values will be compared to the model output as the model only simulates the change of the OCV of the cell. The nomenclature in this paper is that a FOR-branch from discharged to charged state will be e.g. 10% CaD (Charge after Discharge). For a FOR-branch from charged to discharged state the abbreviation DaC (Discharge after Charge) will be used.

For cell type C and D, all measurements were made using a Basytec CTS device. For cell type A and B, a Basytec XCTS device was used. All measurements are conducted inside a controlled climate chamber at the same temperature of $T = 25\ ^\circ\text{C}$. As the OCV points are measured after a minimum of two hours of relaxation, a constant temperature can be ensured. Hence, the effect of OCV change by the entropy of the cell can be excluded.

To measure half-cell potentials of cell type B, experimental cells were built in a three-electrode setup with a Li-ring reference electrode. For this a fresh cell of cell type B was opened in an Ar-filled Glovebox "MB200MOD" (MBraun Inertgas-Systeme GmbH, Germany) with $O_2 < 0.1\,\text{ppm}$ and $H_2O < 0.1\,\text{ppm}$ at 0% SOC. The wounded electrodes were cut into smaller pieces and then washed in dimethyl carbonate bathes two times for five minutes each. After drying, one side of the double-side coated was removed by using n-methyl-2-pyrrolidone (NMP). Afterwards, coins with a diameter of 18 mm were punched out. The coins were then assembled to three-electrode test cells (EL-CELL) with a lithium metal ring reference electrode. With this setup,

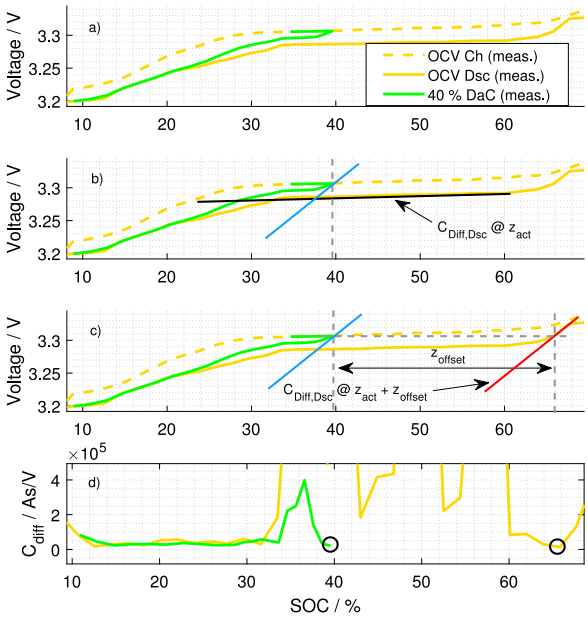

Fig. 3. (a) Exemplary FOR-branch at 40% SOC from charged to discharged state for cell type D. (b) The slope of the measured FOR-branch does not follow the slope of the opposite OCV curve. To demonstrate this, tangential lines (slope of tangential lines equals the differential capacity C_{diff}) were added for the FOR-branch (blue) and for the opposite OCV curve, in this case the discharge OCV curve (black). (c) The slope of the transition correlates strongly with the discharge OCV curve starting at 66% SOC (red and blue lines have the same slope and are only shifted by z_{offset}. (d) Comparison of the differential capacity of the FOR-branch and the discharge OCV curve. The point of the FOR-branch at 40% SOC and the point of the discharge OCV at 66% have the same value. (For interpretation of the references to color in this figure legend, the reader is referred to the web version of this article.)

half-cell potentials of the silicon–graphite composite anode and of the NMC cathode can be measured. All measurement points using the three-electrode setup were also extracted with the same relaxation procedure as for the full-cell tests. For cycling of the experimental cells, the same voltage limits like for the full cell were used so that the balancing of the electrodes does not change.

4. Results and Discussion

4.1. Substituting SOC dependency of the rate of decay-parameter k by using the differential capacity

The first improvement to the presented Plett-model is to use the differential capacity to describe the SOC-dependency of the hysteresis transition. The differential capacity is the slope of the OCV curve defined as:

$$C_{\text{diff}}(z) = \frac{\mathrm{d}Q}{\mathrm{d}U(z)} \tag{5}$$

In this paper, the differential capacity is calculated as a difference quotient in 2%-SOC steps.

Fig. 3(a) shows an exemplary transition for cell D from the charge OCV at 40% to the discharge OCV.

As can be seen in Fig. 3(b) the slope of the FOR-branch is not correlating with the slope of the discharge OCV curve at the current SOC (z_{act} = 40%). This is shown by the insertion of tangential lines at the given SOC. The slope of the blue and the black tangential lines does not match. In Fig. 3(c) it is visible, that the slope of the FOR-branch can be extracted from the discharge OCV curve, at the point, where the current voltage at 40% SOC on the charge OCV curve matches the voltage on the discharge OCV curve. In this case, this point is at 66% SOC. To visualize this, a gray horizontal line is added in Fig. 3(c). At this point, the slope of the discharge OCV curve matches the slope of the FOR-branch (see red and blue tangential lines). Fig. 3(d) shows the comparison of the differential capacities of the FOR-branch and the discharge OCV curve. The plot shows, that the point of the FOR-branch at 40% SOC and the point of the discharge OCV at 66% have nearly the same value. The value will differ a bit as the FOR-branch needs to approach the opposite OCV curve. This can be done for every point on the FOR-branch. For every value of the FOR-branch the corresponding SOC value of the discharge OCV has to be found, where the voltages are equal.

This behavior can also be seen in the publication of Graells et al. [15] in the first figure for a silicon anode.

Therefore, the differential equation in Eq. (4) will be adapted to:

$$\frac{\mathrm{d}h(z,t)}{\mathrm{d}t} = \left(\frac{k(z)\cdot I(t)}{Q_{\text{Cell}}}\right)\left(1-\operatorname{sgn}\left(\frac{\mathrm{d}z(t)}{\mathrm{d}t}\right)h(z,t)\right) \tag{6}$$

with:

$$k(z) = K\cdot\frac{1}{C_{\text{diff}}(z)} \tag{7}$$

This optimization leads to a reduced measurement time, as the SOC-dependency of the parameter K does not need to be fitted anymore to all FOR-branches over the complete SOC-range as it is given by the SOC-dependency of the differential capacity.

As already mentioned, the slope of the FOR-branch has to be taken from discharge OCV not at the actual SOC, but needs to be adapted by an offset. This offset is calculated by an algorithm, which checks at which SOC $U_{\text{OCV,Ch}}(z_{\text{act}}) = U_{\text{OCV,Dsc}}$. In the case of a transition from charge to discharge OCV, the offset is positive, as due to the hysteresis, the discharge OCV has the same OCV voltage at a higher SOC. This leads to the improvement, that the SOC, which will be taken to get the differential capacity, is adapted by an offset:

$$z_{C_{\text{diff}}} = z_{\text{act}} + z_{\text{offset}} \tag{8}$$

The differential equation can then be expressed as:

$$\frac{\mathrm{d}h(z,t)}{\mathrm{d}t} = K\cdot\left(\frac{I(t)}{Q_{\text{Cell}}\cdot C_{\text{diff}}(z)}\right)\left(1-\operatorname{sgn}\left(\frac{\mathrm{d}z(t)}{\mathrm{d}t}\right)h(z,t)\right) \tag{9}$$

To further improve the model, the influence of the differential capacity can be increased by the introduction of an exponent to the differential equation. Therefore, Eq. (7) will be adapted to:

$$k(z) = K\cdot\frac{1}{(C_{\text{diff}}(z))^{x}} \tag{10}$$

with K and x as parameters, which need to be fitted to the FOR-branches. Thereby, the model can be optimized even further.

With the help of this modification the transition can be described in a better way compared to the original Plett-model (see Table 3), which is shown in Fig. 4 for cell type C and D.

It shows one FOR-branch for cell type C and one FOR-branch for cell type D. It can be seen that the modifications also work for cell type C and D, which leads to the conclusion that the modifications work for different cell types and different cell chemistries. For cell type D it is important to note, that due to the low steepness of the LFP-OCV measurement errors can have huge impact on the accuracy of the model.

In Fig. 5 the results of the model optimization is shown for cell type B. Especially for the transition at 10% SOC, the model follows the measured curve better by adapting the rate of decay for every SOC step by using the differential capacity of the OCV. For the transition at 30% SOC, the model does not depict the kink in the transition correctly.

It can be seen that the charge OCV features an earlier kink so that even with the offset-correction of the differential capacity this part of the differential capacity is not taken into account correctly by the model. A possible explanation could be the direction-dependent lithiation/delithiation of the composite materials due to different hysteresis behaviors of both materials. Electrodes containing graphite show

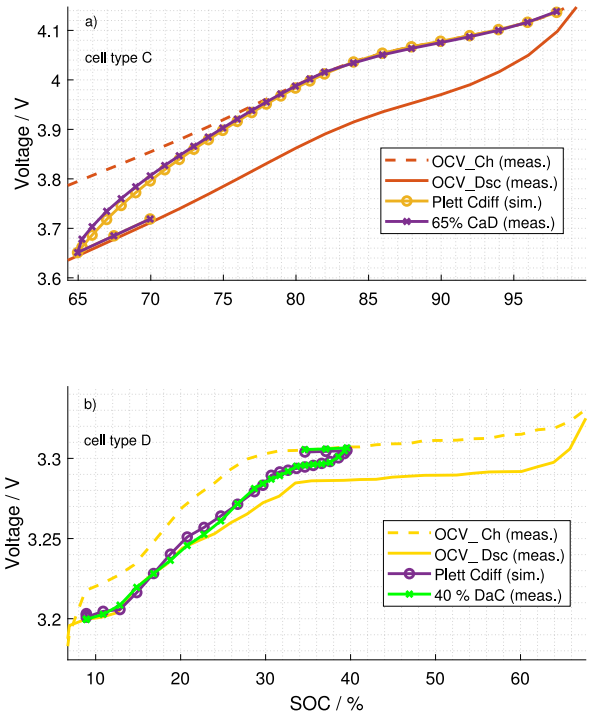

Fig. 4. (a) Exemplary FOR-branch at 65% SOC from discharged to charged state for cell Type C. (b) Exemplary FOR-branch at 40% SOC from charged to discharged state for cell Type D.

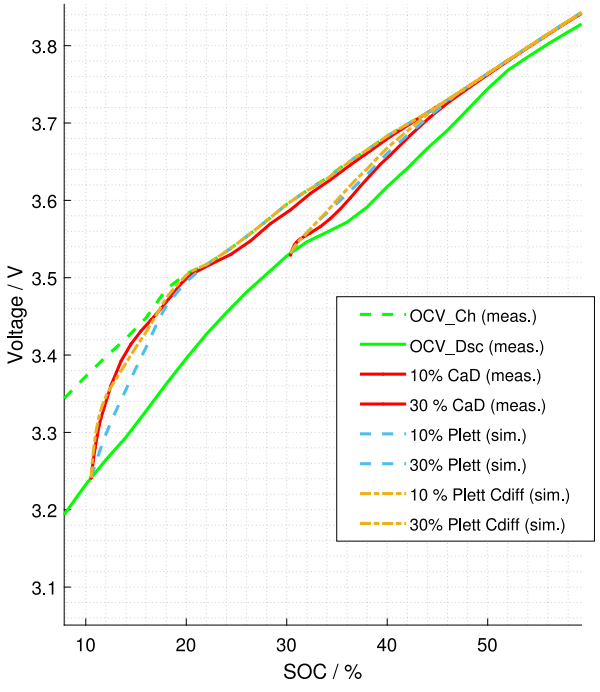

Fig. 5. Exemplary FOR-branches at 10% and 30% SOC from discharged to charged state. The simulated transitions with the different modifications are shown.

multiple voltage plateaus. The plateaus are a result of the staging mechanism of the graphite. In pure graphite, the transition between different voltage plateaus are at a certain concentration (SOC) of the electrode. Due to the asymmetry in lithiation and delithiation of the composite electrode, the voltage plateaus (marked with arrows in Fig. 6) are shifted in SOC in the anode OCV. This SOC-shift leads, due to the steep OCV of the cathode, to a SOC- and full-cell-voltage shift in the full-cell OCV. In non-composite materials, there is no such big shift in SOC between the plateaus/phase transitions. Therefore, for composite-materials, we suggest a simulation of both composite materials independently, as demonstrated in the next section.

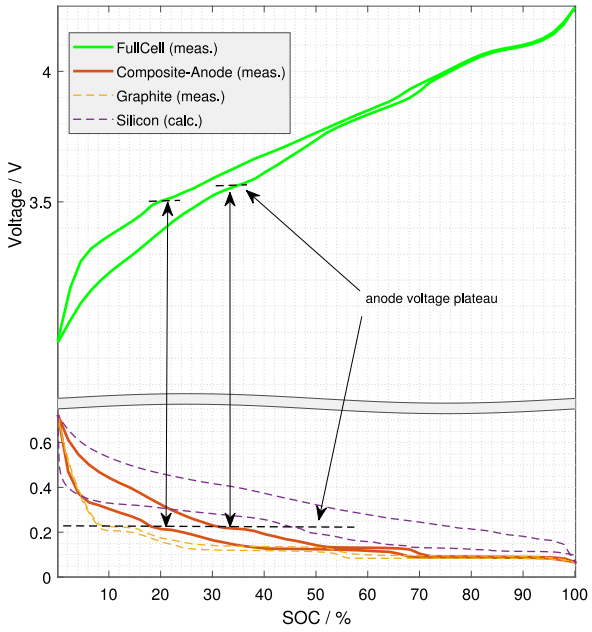

Fig. 6. Comparison of the anode OCV against the full-cell OCV for cell type B. Due to different hysteresis behavior of the composite materials, the voltage plateaus of the anode (marked with arrows and horizontal dashed line) are shifted in SOC in the anode OCV. This SOC-shift leads, due to the steep OCV of the cathode, to a SOC- and full-cell-voltage shift in the full-cell OCV (see voltage difference in dashed horizontal lines).

4.2. Improvement for composite electrode materials

The model improvements also work for composite electrodes like cell type B (see Fig. 5, 10% CaD) except for minor difficulties (see Fig. 5, 30% CaD). To further improve the accuracy of the model, the separation of both materials in the anode is suggested. Therefore, the hysteresis of the anode will be simulated with a parallel connection of silicon and graphite. In this case, the model complexity is kept as small as possible. For the sake of simplicity, overpotentials due to the current-flow, are being neglected. If the properties of both materials differ from each other, the current distribution would change. It is reported in literature, that silicon exhibits slow solid-state diffusion [29], but the overpotentials are also dependent on the geometry of the different materials. Often silicon particles are smaller than graphite particles, which improves the kinetic behavior. The measurements shown in this paper were conducted with C/10 and the incremental steps of the shown FOR-branches were relatively low (<= 1%). After each step, a redistribution of lithium occurs, as the overpotentials decrease [30]. While an external current flows, the graphite particles would be more lithiated/delithiated than the silicon particles, due to the higher overpotentials in the silicon. After the external current stops, the overpotentials of both materials decrease. As the OCV of the graphite particles changed more, than the OCV of the silicon particles, a potential difference between both materials will still be present. This potential difference will be balanced by the redistribution. For the case of lithiation, the graphite particles will be delithiated and the silicon will be further lithiated until the potential difference is zero. By neglecting the hysteresis behavior of the graphite, which can be assumed as the amount of charge transferred during the redistribution

Table 3
Comparison of the error for the different improvements made to the original Plett-model for cell B. Please note that the calculated error strongly depends on the choice of the transition steps. As shown, the improvements lead to a significant change in the transitions especially during phase transformations.

Modification	RMS/mV	Improve./%
Original Plett	7.05	0
Plett C_{diff}	6.75	4.3
Plett $(C_{\text{diff}})^{1.4}$	6.65	5.6
SiGr separated C_{diff}	5.45	22.7
SiGr separated $(C_{\text{diff}})^{1.4}$	4.65	34.1

will be rather low when the complete SOC step was only <= 1%, the current distribution should follow the differential capacities of silicon and graphite [30].

For a constant charge or discharge cycle, or a varying current-profile with higher C-rates, overpotentials should be taken into account, to track the lithiation/delithiation of both materials correctly.

However, for the model, the OCVs of both anode materials have to be known. As there is no possibility to measure the OCV of both materials of the composite electrode independently, the OCV of the silicon material is calculated using the measured composite-OCV by assuming that even for an unknown graphite material, the OCV of the graphite can be taken from other cells as the OCV variation of different graphite materials can be neglected in comparison to the hysteresis of the silicon materials. With the graphite OCV and the measured anode OCV, the silicon OCV can be calculated using differential voltage analysis (DVA) fitting [31].

The full cell current I_{total} is then split into a current for the graphite I_{Gr} and for the silicon I_{Si} so that the voltages U_{Gr} and U_{Si} are equal:

$$U_{\text{Gr,i}-1} + I_{\text{Gr,i}} \cdot \frac{1}{C_{\text{diff,Gr}}} \cdot t_{\text{s}} = U_{\text{Si,i}-1} + I_{\text{Si,i}} \cdot \frac{1}{C_{\text{diff,Si}}} \cdot t_{\text{s}} \tag{11}$$

$$I_{\text{total,i}} = I_{\text{Gr,i}} + I_{\text{Si,i}} \tag{12}$$

These equations can be used to determine both lithiation/delithiation currents $I_{\text{Gr,i}}$ and $I_{\text{Si,i}}$ for each time step i with the step time of t_{s}. $U_{\text{Gr,i}}$ respectively $U_{\text{Si,i}}$ are calculated by Eq. (1) with the above mentioned improvements for the Plett-model. The change in voltage of the materials is calculated by the current multiplied with the differential capacity at the current SOC. The small change in hysteresis over one simulation step can be neglected for a small step-size (t_{s} = 0.02 s in this case). The resulting hysteresis transitions compared to the measurements can be seen in Fig. 7.

The difference between the optimized full cell and the optimized separated composite electrode model can be seen best for 30% as the full cell model does not feature the kink in the transition correctly. Also, for the transition at 10% SOC, the improvement shows a better result as the transition takes a longer amount of charge, which fits the measurement better.

In Table 3, the mean deviation between measurements of the FOR-branches (in 10% SOC-steps) in the complete operating window of cell B against the simulation is shown. The mean deviation of the model was calculated as the sum of the amount of deviation at the individual measuring points divided by the number of measuring points. The most significant improvement can be gained by separating the hysteresis model into anode and cathode, with separation of the composite anode itself. Nevertheless, the improvement by using the differential capacity is better than the original Plett-model.

4.3. Ageing behavior of the hysteresis transition

Another important aspect concerning the application of hysteresis modeling in Li-ion batteries is cell ageing. Fig. 8 shows a comparison

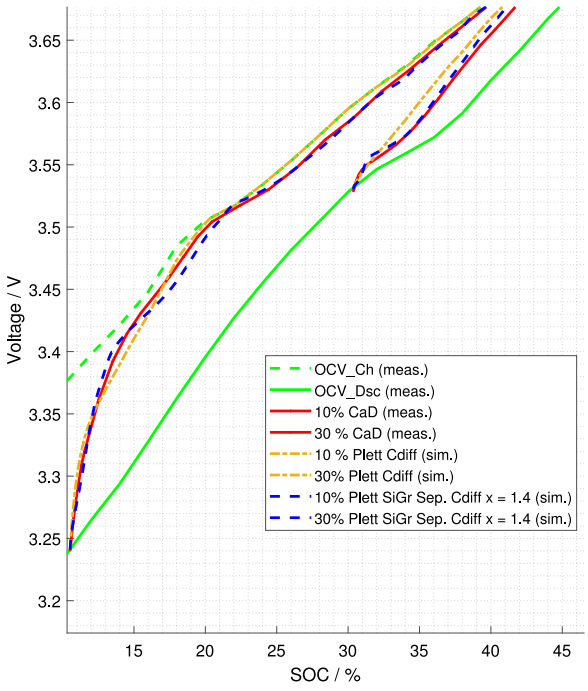

Fig. 7. Exemplary FOR-branch at 10% and 30% SOC from discharged to charged state. The simulated transition with the separated composite electrode model against the full cell model is shown.

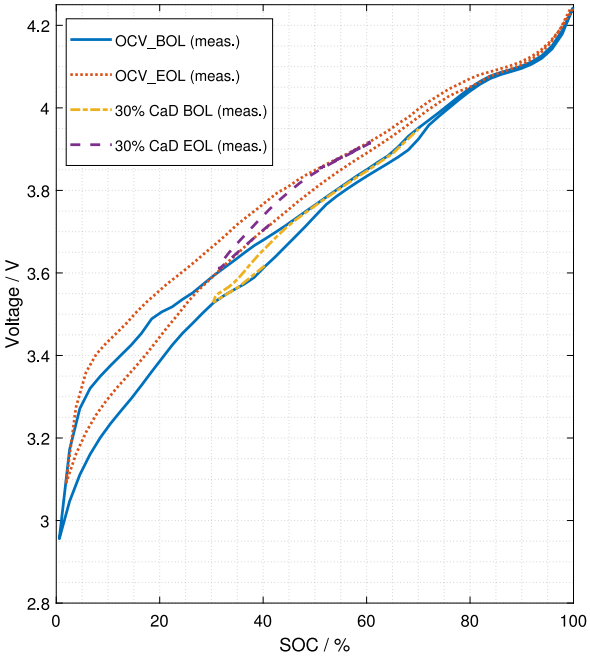

Fig. 8. Comparison of the hysteresis transition for Cell type B at different SOH. The slope of the transition changes with ageing of the cell. However, it still follows the slope of the measured OCV curves. The SOC was calculated for each cell individually.

of a fresh cell of cell type B and an aged cell at an SOH (capacity-based) of 77%.

Additionally, the same hysteresis transition at the same SOC is shown. Note, that the same SOC does not mean that the concentration inside the electrodes needs to be the same. Due to the ageing, the balancing of the electrodes can be different. It can be seen that the progression of the slope of the transition changes with ageing, which

would lead to wrong hysteresis modeling without our proposed improvements if the parameters for the rate of decay were not changed. As the figure shows, though, even for aged cells, the slope of the transition follows the slope of the OCV curves, in this case the aged OCV curve. This leads to the fact that with our model, there is no need to change the parameters if the OCV and therefore the differential capacity of the aged cell is known. As the complete transition between both OCV curves takes the same amount of charge, the parameter K out of Eq. (10) does not need to be changed.

5. Conclusion

In this article, improvements to the original presented hysteresis model by Plett et al. [10–13,15] are presented. It was shown that information about the transition between the hysteresis states can be gathered from the OCV curves itself. Measurements show, that the differential capacity of the hysteresis transition is not SOC—but voltage-dependent. Therefore, the SOC-dependency of the rate of decay was adapted to take account of the differential capacity. By the exponentiation of the differential capacity, the influence of the slope of the OCV on the transition can be increased even further. The improvements lead to less effort for parameterization, as the SOC-dependency of the transition does not have to be fitted to measurement data, which also reduces the measurement time significantly. Furthermore, an improvement for composite electrodes was shown by modeling the hysteresis of both materials independently. The accuracy of the model is strongly dependent on the quality of the measurement, on half-cell level in particular. Therefore, future work should investigate how to improve the measurement quality to ensure a better model quality. It was shown that this modeling approach is also valid for aged cells. The modeling approach therefore further reduces the parameterization process. For further studies, the shown effect, that the hysteresis transition is voltage-driven not SOC-driven, can be used to further investigate the hysteresis behavior of Li-ion cells.

CRediT authorship contribution statement

Dominik Wycisk: Conceptualization, Methodology, Validation, Visualization, Writing. **Marc Oldenburger:** Conceptualization, Methodology. **Marc Gerry Stoye:** Methodology, Validation. **Toni Mrkonjic:** Conceptualization, Reviewing. **Arnulf Latz:** Supervision, Reviewing.

Declaration of Competing Interest

The authors declare that they have no known competing financial interests or personal relationships that could have appeared to influence the work reported in this paper.

References

[1] J. Lyubina, Phase transformations and hysteresis in Si-based anode materials, Appl. Phys. Lett. (2020).
[2] M.N. Obrovac, V.L. Chevrier, Alloy Negative Electrodes for Li-Ion Batteries, Chem. Rev. (2014).
[3] M.N. Obrovac, L.J. Krause, Reversible Cycling of Crystalline Silicon Powder, J. Electrochem. Soc. (2006).
[4] W. Dreyer, C. Guhlke, R. Huth, The behavior of a many-particle electrode in a lithium-ion battery, Physica D (2011).
[5] Z. Xu, J. Wang, Q. Fan, P.D. Lund, J. Hong, Improving the state of charge estimation of reused lithium-ion batteries by abating hysteresis using machine learning technique, J. Energy Storage (2020).
[6] C.Y. Chun, B.H. Cho, J. Kim, Covariance controlled state-of-charge estimator of LiFePO4 cells using a simplified hysteresis model, Electrochim. Acta (2018).
[7] I.D. Mayergoyz, Mathematical Models of Hysteresis, Springer, 1991.
[8] F. Baronti, N. Femia, R. Saletti, C. Visone, W. Zamboni, Preisach modelling of lithium-iron-phosphate battery hysteresis, J. Energy Storage (2015).
[9] P. Chayratsami, G.L. Plett, Hysteresis modeling of lithium–silicon half cells using extended Preisach model, in: 15th International Conference on Control, Automation, Robotics and Vision, ICARCV, IEEE, 2018.
[10] G.L. Plett, Advances in EKF SOC estimation for LiPB HEV battery packs, in: CD-ROM Proc. 20th Electric Vehicle Symposium, EVS20, 2003.
[11] G.L. Plett, Extended Kalman filtering for battery management systems of LiPB-based HEV battery packs: Part 2. modeling and identification, J. Power Sources (2004).
[12] G.L. Plett, Battery management systems, in: Volume I: Battery Modeling, Artech House, 2015.
[13] G.L. Plett, Battery management systems, in: Volume II: Equivalent-Circuit Methods, Artech House, 2015.
[14] X. Xiao D.R. Baker, An approach to characterize and clarify hysteresis phenomena of lithium-silicon electrodes, J. Appl. Phys. (2017).
[15] C. Graells, S. Trimboli, G. Plett, Differential hysteresis models for a silicon-anode Li-ion battery cell, in: IEEE Transportation Electrification Conference & Expo, ITEC, 2020.
[16] M. Oldenburger, B. Beduerftig, A. Gruhle, F. Grimsmann, E. Richter, Investigation of the low frequency Warburg impedance of Li-ion cells by frequency domain measurements, J. Energy Storage (2019).
[17] F. Grimsmann, F. Brauchle, T. Gerbert, A. Gruhle, M. Knipper, J. Parisi, Hysteresis and current dependence of the thickness change fo lithium-ion cells with graphite anode, J. Energy Storage (2017).
[18] A. Van der Ven, Z. Deng, S. Banerjee, S.P. Ong, Rechargeable Alkali-Ion Battery Materials: Theory and Computation, Chem. Rev. (2020).
[19] F.M. Kindermann, A. Noel, S. Erhard, A. Jossen, Long-term equalization effects in Li-ion batteries due to local state of charge inhomogeneities and their impact on impedance measurements, Electrochim. Acta (2015).
[20] T. Huefner, M. Oldenburger, B. Beduerftig, A. Gruhle, Lithium flow between active area and overhang of graphite anodes as a function of temperature and overhang geometry, J. Energy Storage (2019).
[21] I. Zilbermann, S. Ludwig, A. Jossen, Cell-to-cell variation of calendar aging and reversible self-discharge in 18650 nickel-rich, silicon-graphite lithium-ion cells, Electrochim. Acta (2019).
[22] M.P. Mercer, C. Peng, C. Soares, H.E. Hoster, D. Kramer, Voltage hysteresis during lithiation/delithiation of graphite associated with meta-stable carbon stackings, J. Mater. Chem. A (2021).
[23] V. Srinivasan, J. Newman, Discharge Model for the Lithium Iron-Phosphate Electrode, J. Electrochem. Soc. (2015).
[24] V.A. Sethuraman, V. Srinivasan, A.F. Bower, P.R. Guduru, In Situ Measurements of Stress-Potential Coupling in Lithiated Silicon, J. Electrochem. Soc. (2010).
[25] Y. Jiang, G. Offer, J. Jiang, M. Marinescu, H. Wang, Voltage Hysteresis Model for Silicon Electrodes for Lithium Ion Batteries, Including Multi-Step Phase Transformations, Crystallization and Amorphization, J. Electrochem. Soc. (2020).
[26] V.L Chevrier, J.R. Dahn, First Principles Studies of Disordered Lithiated Silicon, J. Electrochem. Soc. (2010).
[27] C.R. Birkl, E. McTurk, M.R. Roberts, P.G. Bruce, D.A. Howey, A Parametric Open Circuit Voltage Model for Lithium Ion Batteries, J. Electrochem. Soc. (2015).
[28] A. Barai, W. Dhammika Widanage, J. Marco, A. McGordon, P. Jennings, A study of the open circuit voltage characterization technique and hysteresis assessment of lithium-ion cells, J. Power Sources (2015).
[29] K. Pan, F. Zou, M. Canova, Y. Zhu, J.H. Kim, Systematic electrochemical characterizations of Si and SiO anodes for high-capacity Li-Ion batteries, J. Power Sources (2019).
[30] C. Heubner, T. Liebmann, O. Lohrberg, S. Cangaz, S. Maletti, A. Michaelis, Understanding Component-specific Contributions and Internal Dynamics in Silicon/Graphite Blended Electrodes for High-Energy Lithium-Ion Batteries, Batter. Supercaps (2021).
[31] K.P.C. Yao, J.S. Okasinski, K. Kalaga, J.D. Almer, D.P. Abraham, Operando Quantification of (De)Lithiation Behavior of Silicon-Graphite Blended Electrodes for Lithium-Ion Batteries, Adv. Energy Mater. (2019).